A PHASE SCREEN SIMULATOR FOR PREDICTING THE IMPACT OF SMALL-SCALE IONOSPHERIC STRUCTURE ON SAR IMAGE FORMATION AND INTERFEROMETRY

Charles S. Carrano[1], Keith M. Groves[2], and Ronald G. Caton[3]

[1]Institute for Scientific Research, Boston College, Boston, MA
[2]Air Force Research Laboratory, Hanscom AFB, MA
[3]Air Force Research Laboratory, Kirtland AFB, NM

ABSTRACT

We describe the SAR Scintillation Simulator (SAR-SS), a new phase screen model for simulating the impact of small-scale ionospheric structure on SAR image formation and interferometry. We compare simulated and observed PALSAR imagery over Brazil, and our preliminary findings show that SAR-SS can reproduce the essential features of azimuthal streaking and contrast degradation caused by small-scale structure in the ionosphere.

Index Terms— Radio Scintillation, Synthetic Aperture Radar, Ionospheric Irregularities

1. INTRODUCTION

The effects of the ionosphere on synthetic aperture radar (SAR) can be categorized into two different types [11]. The first type consists of effects caused by the ionospheric background such as refraction, polarization rotation, group delay, and phase advance. These effects can be largely mitigated for an L-band SAR if a suitable model for the ionosphere is employed during SAR processing [2]. The second type consists of effects caused by small-scale ionospheric structures which are generated by plasma instability processes. These instability processes act predominantly in the polar cap and equatorial zone at night, the effects being more pronounced during periods of high solar activity. As radio waves penetrate these small-scale structures, they randomly scatter in different directions resulting in spatial variations in signal phase. These phase variations cause interference as the radio wave propagates further in free-space, resulting in a diffraction pattern on the ground with spatial fluctuations in both amplitude and phase. These signal fluctuations are intensified as the reflected wave traverses the ionosphere a second time after reflection from the ground. Amplitude and phase fluctuations which decorrelate across the synthetic aperture of the radar reduce the effective resolution of a SAR image, and alter critical differential phase relationships between images collected during satellite revisits that are required by InSAR and change detection applications.

In this paper we present a new phase screen model called the SAR Scintillation Simulator (SAR-SS) for predicting the impact of small-scale ionospheric structure on SAR image formation and interferometry. This simulator consists of a phase screen generator and a propagator. The screen generator creates a 2D random realization of spatial phase fluctuations resulting from the traversal of small-scale irregularities in the ionosphere. The irregularities are specified statistically in terms of a power spectral density that depends on 1) the vertically integrated strength of turbulence, 2) the spectral index, 3) the outer scale, and 4) the anisotropy ratio along and transverse to the local magnetic field direction. The screen generator accounts for the motion of the radar platform, the drift of the ionospheric irregularities, and the oblique angle of propagation, all of which determine the scale sizes of the irregularities sampled by the radar beam. The statistical parameters specifying the irregularities can be input to the simulator manually, or provided by the Wideband ionospheric scintillation model (WBMOD), a global climatological model of scintillation constructed from an extensive database of observations [10].

The propagator of the SAR-SS model solves the 3D parabolic wave equation (PWE) using the split-step technique to compute the diffraction pattern of amplitude and phase at the radar caused by two-way propagation through the ionosphere. This diffraction pattern can used to modulate the SAR signal due to terrestrial features in order to assess the ionospheric impact on SAR image formation and interferometry. We note that SAR-SS is similar in many respects to a previous phase screen model called SAR-TIRPS [9], except that the later was constructed using a 1D phase screen. The SAR-SS model uses a 2D phase screen which facilitates the simulation of 2D SAR images.

The outline of this paper is as follows. In sections 2 and 3 we present the propagator and phase screen generator of the SAR-SS model, respectively. Section 4 shows an application of the model whereby the effects of small-scale irregularities in the ionosphere are added to a PALSAR L-

band SAR image collected during quiet ionospheric conditions, and the results are compared with a PALSAR image collected during a revisit over the same terrain during disturbed ionospheric conditions.

2. SPLIT-STEP SOLUTION OF THE PARABOLIC WAVE EQUATION

The scalar Helmholtz equation governs the propagation of radio waves through a weakly inhomogeneous media in the absence of currents and depolarization effects:

$$\nabla^2 E(\mathbf{r}) + k^2 n^2 E(\mathbf{r}) = 0 \tag{1}$$

In the above, $E(\mathbf{r})$ is the electric field, n is the index of refraction, and $k=2\pi/\lambda$ where λ is the wavelength of the radio wave. The $e^{i2\pi ft}$ dependence is implied, where f is the frequency. We define the reduced electric field $U(\mathbf{r})$ as

$$E(\mathbf{r}) = U(\mathbf{r}) e^{i\mathbf{k}\cdot\mathbf{r}} \tag{2}$$

in order to remove the oscillatory component of the field along the propagation direction. The coordinate system chosen for the propagation calculation is shown in Figure 1. The origin is located at the ionospheric penetration point (IPP) along the propagation path at the center of the radar beam. The x, y, and z axes point toward geomagnetic north, geomagnetic east, and vertically downward, respectively. The thickness of the ionospheric layer, assumed to contain homogeneously distributed irregularities, is L.

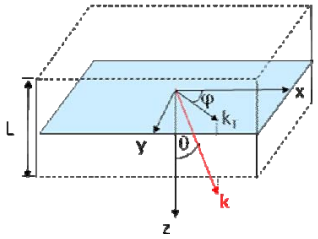

Figure 1. The propagation coordinate system centered at the IPP.

In this coordinate system, the wavevector is given by

$$\mathbf{k} = \frac{2\pi}{\lambda}(\sin\theta\cos\varphi, \sin\theta\sin\varphi, \cos\theta) \tag{3}$$

Substituting (2) and (3) into (1), and assuming the medium changes sufficiently slowly in the direction of propagation, yields a form of the PWE for the reduced field where the propagation angles appear explicitly:

$$\frac{\partial^2 U}{\partial x^2} + 2ik\sin\theta\cos\varphi\frac{\partial U}{\partial x} + \frac{\partial^2 U}{\partial y^2} + 2ik\sin\theta\sin\varphi\frac{\partial U}{\partial y} + 2ik\cos\theta\frac{\partial U}{\partial z} + 2k^2\Delta n U = 0 \tag{4}$$

In (4), Δn is the fluctuating part of the index of refraction, which assumed to be small (an additional term of order Δn^2 has been neglected).

We solve equation (4) using the split-step approach [5]. Inside the scattering layer we neglect the diffraction terms which involve second derivatives of U. In the high frequency limit (geometric optics), the phase change imparted by the ionosphere is proportional to the integral of electron density fluctuations ΔN_e along the line of sight [7]:

$$\begin{aligned}\phi(\boldsymbol{\rho}) &= k\int_{-L/2(\sec\theta)}^{L/2(\sec\theta)} \Delta n(\mathbf{r})\,dl \\ &= \lambda r_e \sec\theta \int_{-L/2}^{L/2} \Delta N_e(\boldsymbol{\rho} + \tan\theta\,\hat{a}_{k_T}(\eta - z), \eta)\,d\eta\end{aligned} \tag{5}$$

where $\boldsymbol{\rho}$ is a distance vector in the horizontal plane, $\hat{a}_{k_T} = (\cos\varphi, \sin\varphi)$ is a unit vector in the horizontal plane, and r_e is the classical electron radius. We neglect refraction effects and assume the propagation path is a straight line. The reduced electric field after single passage through the phase screen is then $U(\boldsymbol{\rho},\mathbf{0}^+) = U(\boldsymbol{\rho},\mathbf{0})e^{i\phi(\boldsymbol{\rho})}$.

After the radio wave has passed through the screen, we neglect index of refraction fluctuations and solve (4) for the reduced electric field after propagation through free space. It is convenient to seek a solution to (4) in terms of the transverse Fourier transform of U which is defined as

$$U(\boldsymbol{\rho}, z) = \frac{1}{(2\pi)^2}\int_{-\infty}^{\infty}\int_{-\infty}^{\infty} \hat{U}(\boldsymbol{\kappa}, z)\, e^{i\boldsymbol{\kappa}\cdot\boldsymbol{\rho}}\, d\boldsymbol{\kappa} \tag{6}$$

where $\boldsymbol{\kappa}$ is the transverse wavenumber. This procedure yields the following solution for the reduced field after single passage through the phase screen:

$$U(\boldsymbol{\rho}, z) = \frac{1}{(2\pi)^2}\int_{-\infty}^{\infty}\int_{-\infty}^{\infty} \hat{U}(\boldsymbol{\kappa}, 0^+)\cdot \exp\left[-i\left(\frac{\kappa^2}{2k} z\sec\theta + (\hat{a}_{k_T}\cdot\boldsymbol{\kappa}) z\tan\theta\right)\right] e^{i\boldsymbol{\kappa}\cdot\boldsymbol{\rho}}\, d\boldsymbol{\kappa} \tag{7}$$

Equation (7) gives the split-step solution to (4) subject to the thin screen approximation for the case of an incident monochromatic plane wave. Following Rino [8], the SAR-SS model (optionally) applies a correction to account for spherical curvature of the radio wave by scaling the transverse coordinates x and y, and the also the propagation distance, by $z_1/(z_1+z_2)$ where z_1 is the slant distance (not the vertical distance) from the radar to the IPP and z_2 is the slant distance from the IPP to the center of the target area. In this case the reduced electric field on the ground can be expressed as [1]

$$U\left(\frac{z_1}{z_1+z_2}\boldsymbol{\rho}, z_2\right) = U_0\left(\frac{z_1}{z_1+z_2}\boldsymbol{\rho}, z_2\right) D(\boldsymbol{\rho}) \tag{8}$$

where U_0 is the transmitted monochromatic wave and $D(\boldsymbol{\rho})$ is the ionospheric transfer function which is given by:

$$D(\boldsymbol{\rho}) = F^{-1}\left\{\exp\left[i\frac{\kappa^2}{2k}\left(\frac{z_1}{z_1+z_2}\right)z_2\right] F\left\{e^{i\phi(\boldsymbol{\rho})}\right\}(\boldsymbol{\kappa})\right\} \tag{9}$$

In (9), F denotes the transverse Fourier Transform which can be evaluated efficiently using the fast Fourier transform (FFT) in two dimensions. Note that we have dropped the term $(\hat{a}_{k_T}\cdot\boldsymbol{\kappa})z\tan\theta$ in (7) which translates the reduced field horizontally. This term vanishes in a coordinate system that moves with the IPP.

By symmetry, the ionospheric transfer function is the same for both the downward and upward paths of the radio wave [9]. Therefore, we account for two-way propagation through the ionosphere by squaring $D(\boldsymbol{\rho})$. The reduced field that returns to the horizontal plane of the radar when transmitting a pulse P of bandwidth B, after double passage through the ionosphere, can be expressed [5]:

$$U_r(\boldsymbol{\rho},\tau) = \int_{-\frac{B}{2}}^{\frac{B}{2}} \hat{P}(f) D^2(\boldsymbol{\rho},f)\, e^{2\pi i f \tau}\, df \qquad (10)$$

The above is the integral of the Fourier transform of the pulse, $\hat{P}(f)$, modulated by the ionospheric transfer function for two-way propagation over all frequencies in the pulse. For narrow-bandwidth systems such as PALSAR (28 MHz), we may approximate the pulse as a monochromatic wave at the center frequency, i.e. $\hat{P}(f) = \delta(f_c)$, so that:

$$U_r(\boldsymbol{\rho}) = D^2(\boldsymbol{\rho}, f_c) \qquad (11)$$

3. CONSTRUCTION OF THE PHASE SCREEN

We assume Rino's form for the power spectral density of phase after one-way passage through the phase screen [8]:

$$\Phi_\phi(\boldsymbol{\kappa}) = \frac{\lambda^2 r_e^2 \sec^2\theta\, ab\left(2\pi/1000\right)^{p+1} C_k L}{\left(q_0^2 + A\kappa_x^2 + B\kappa_x\kappa_y + C\kappa_y^2\right)^{(p+1)/2}} \qquad (12)$$

In (12), p is the phase spectral index, a and b are scaling factors that elongate contours of constant correlation along and transverse to the magnetic field, respectively, q_0 is the outer scale wavenumber, and C_kL is the vertically integrated strength of turbulence at the 1 km scale. The coefficients A, B, and C depend on the direction of propagation and the magnetic field and are obtained by relating the radar line of sight and the irregularity axes [8]:

$$\begin{aligned} A &= C_{11} + C_{33}\tan^2\theta\cos^2\varphi - 2C_{13}\tan\theta\cos\varphi \\ B &= 2\left[C_{12} + C_{33}\tan^2\theta\sin\varphi\cos\varphi\right. \\ &\quad \left. - \tan\theta\left(C_{13}\sin\varphi + C_{23}\cos\varphi\right)\right] \\ C &= C_{22} + C_{33}\tan^2\theta\sin^2\varphi - 2C_{23}\tan\theta\sin\varphi \end{aligned} \qquad (13)$$

where

$$\begin{aligned} C_{11} &= a^2\cos^2\psi + \sin^2\psi\left(b^2\sin^2\delta + \cos^2\delta\right) \\ C_{22} &= b^2\cos^2\delta + \sin^2\delta \\ C_{33} &= a^2\sin^2\psi + \cos^2\psi\left(b^2\sin^2\delta + \cos^2\delta\right) \\ C_{12} &= \left(b^2 - 1\right)\sin\psi\sin\delta\cos\delta \\ C_{13} &= \left(a^2 - b^2\sin^2\delta - \cos^2\delta\right)\sin\psi\cos\psi \\ C_{23} &= -\left(b^2 - 1\right)\cos\psi\sin\delta\cos\delta \end{aligned} \qquad (14)$$

In (14), ψ is the magnetic inclination angle and δ is the angle at which irregularities are inclined from the xz plane (typically taken to be zero at low latitudes). SAR-SS obtains the magnetic field parameters at the IPP location from the International Geomagnetic Reference Field [6].

For a right-looking stripmap SAR system with zero squint angle, an appropriate spatial sampling in the geomagnetic east and north directions to use when generating a realization of the random phase screen is:

$$\begin{aligned} \Delta x_e &= \left| \frac{V_{ipp} - V_{De}}{PRF}\sin\left(\varphi - \tfrac{\pi}{2}\right) + \frac{c}{2PSF}\sin(\varphi)/\sin(\gamma) \right| \\ \Delta x_n &= \left| \frac{V_{ipp} - V_{Dn}}{PRF}\cos\left(\varphi - \tfrac{\pi}{2}\right) + \frac{c}{2PSF}\cos(\varphi)/\sin(\gamma) \right| \end{aligned} \qquad (15)$$

In the above, V_{ipp} is the velocity of the IPP, γ is the radar incidence angle at the screen, PRF is the pulse repetition frequency, and PSF is the pulse sampling frequency. To derive (15) we have assumed frozen-in motion of the plasma with eastward and northward components given by V_{De} and V_{Dn}, respectively, and we have neglected Earth rotation. For a right-looking stripmap SAR with zero squint angle, φ-π/2 is the magnetic heading of the radar platform while φ is the magnetic heading of the radar beam. The factor $\sin(\gamma)$ accounts for range foreshortening by converting the range sample spacing $c/(2PSF)$ to equivalent horizontal sample spacing at the phase screen. The spherical wave correction described earlier is (optionally) applied to this grid spacing prior to generating a realization of the phase screen, and then the screen is rotated into alignment with the along-track and range directions of the radar.

4. SIMULATING THE IONOSPHERIC IMPACT ON SAR IMAGES

Equations (10) and (11) give the reduced field at the radar after double passage through the ionosphere in the absence of terrestrial features on the ground (as if the ground were a perfect mirror). The SAR-SS model predicts the impact of the ionosphere on SAR imagery by replacing the transmitted radar pulse P with the received SAR signal (e.g. unfocused complex phase history) in (11). This effectively assumes the terrain consists of frequency-flat point scatterers at each pixel location which contribute independently to the SAR signal. For this study, we began with single look complex (SLC) data from PALSAR and simulated the unfocused SAR signal by applying the range-Doppler algorithm (RDA) in reverse [4]. We could have skipped this inversion step and used the raw unfocused SAR signal directly, but this data was not available at the time of this study. We modulated this simulated unfocused SAR signal with the ionospheric transfer function $D^2(\boldsymbol{\rho})$, and applied the RDA algorithm in the forward sense [3] to produce a simulated SAR image with ionospheric effects added.

Before demonstrating the application of the SAR-SS model, we first show PALSAR imagery during two consecutive revisits over the same ground terrain in Brazil. Figure 2 shows a sub-look image on 25 December 2007 during quiet ionospheric conditions and Figure 3 shows a sub-look of the same terrain on 26 March 2008 when the ionosphere was disturbed. Note the loss of contrast and prominent streaks in the 26 March image along the direction of the geomagnetic field, indicated by the arrow. These streaks are inclined at approximately -5.7°, which is the radar magnetic heading at this location.

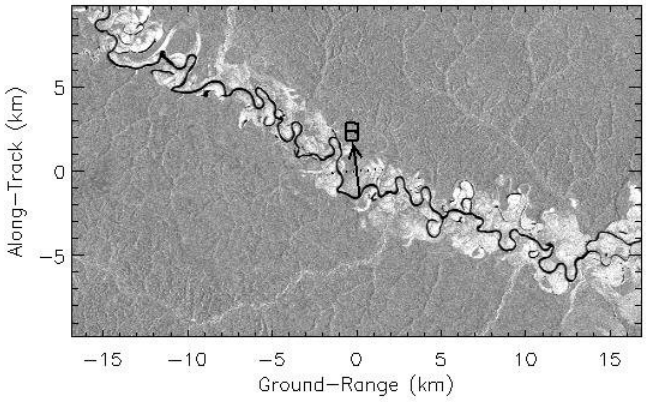

Figure 2. PALSAR sub-look image on 25 December 2007 during quiet ionospheric conditions.

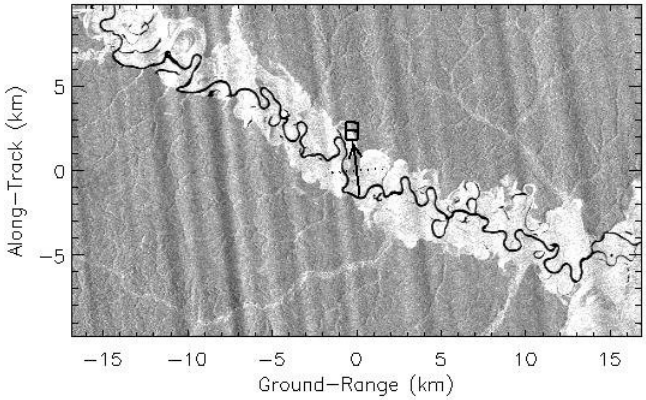

Figure 3. PALSAR sub-look on 26 March 2008 showing evidence of ionospheric streaking.

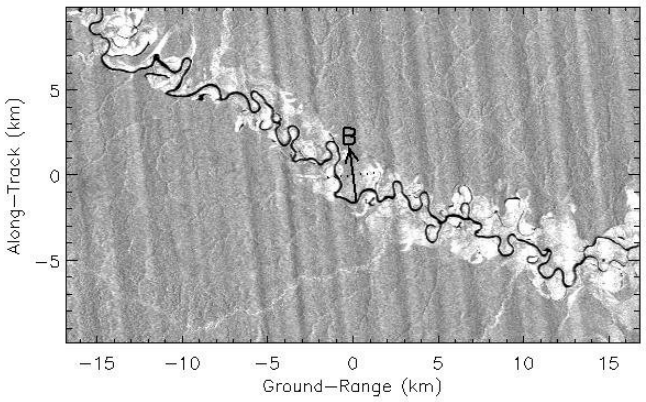

Figure 4. Simulated PALSAR observation obtained by imposing ionospheric effects on the image shown in Figure 2.

We applied the SAR-SS model to the PALSAR data on 25 December 2007 by generating a phase screen based on the radar location and magnetic field parameters at the IPP, and then modulating the SAR signal to account for two-way propagation through the screen. The resulting image is shown in Figure 4. The following parameters were used in this simulation: scene center (-4.05°,-67.91°), radar heading 348°, magnetic declination -5.7°, magnetic inclination 14.4°, a:b=50:1, $C_kL=10^{34}$, $2\pi/q_0$=10km, p=6.0, no spherical wave correction. The qualitative similarity between the observed PALSAR image (Figure 3) and the simulated image (Figure 4) suggests the SAR-SS model can reproduce the essential features of azimuthal streaking and contrast degradation caused by small-scale structure in the ionosphere.

Our numerical experiments suggest that a phase spectral index of 6 approximately reproduces the spacing between the streaks observed on 26 March 2008. This rather steep index suggests the ionospheric irregularities that caused the streaks may be better characterized by a Gaussian, rather than a power-law, spectrum. Alternatively, it may suggest that our screen generator did not faithfully represent the largest scale features of the turbulence, given that the dimensions of our sub-look image are too small to resolve the 10 km outer scale. These results should be considered preliminary, as additional analysis needs to be performed on both the observed and simulated images to validate the results.

ACKNOWLEDGEMENTS

The authors thank David Belcher and Neil Rogers for their helpful comments on SAR modeling, Franz Meyer for providing the PALSAR data, and User Systems who extracted the imagery. This work was sponsored by Air Force contract FA8718-09-C-0041.

REFERENCES

[1] Bernhardt, P., et al., "Ionospheric applications of the scintillation and tomography receiver in space mission when used with the DORIS radio beacon network," *J. Geod*, 80, 2006.

[2] Chapin, E., et al., "Impact of the ionosphere on an L-band space based radar," Radar, 2006 IEEE Conf., 24–27, 2006.

[3] Cumming, I. and J. Bennett, "Digital processing of SEASAT SAR data," Internal Conference on Acoustics, Speech and Signal Processing, IEEE, Washington, D. C., April 1979.

[4] Khwaja, A., L. Ferro-Famil, and E. Pottier, "SAR raw data simulation using inverse SAR image formation algorithms," in Proc. IGARSS, 2006, 4191–4194.

[5] Knepp, D., L. Nickisch, "Multiple phase screen calculation of wide bandwidth propagation," *Radio Sci*., 44, RS0A09, doi:10.1029/2008RS004054, 2009.

[6] Olsen, N., T. Sabaka, and L. Tøffner-Clausen, "Determination of the IGRF 2000 model," *Earth Planets Space*, 52, 1175–1182, 2000.

[7] Rino, C., E. Fremouw, "The angle dependence of singly scattered wavefields," *J. Atmos. Terr. Phys*., 39, 859-868, 1977.

[8] Rino, C., "A power law phase screen model for ionospheric scintillation,1 Weak scatter," *Radio Sci*, 14, 1135-1145, 1979.

[9] Rogers, N., P. Cannon, "The synthetic aperture radar trans-ionospheric radio propagation simulator (SAR-TIRPS)," IRST 2009 Conf., 28-30 April 2009, Edinburgh, pp. 112-116.

[10] Secan, J., R. Bussey, E. Fremouw, S.A. Basu, "An improved model of equat. scint.," *Radio Sci*., 30, (3), 607–617, 1995.

[11] Xu, Z.-W., J. Wu, Z.-S. Wu, "A survey of ionospheric effects on space-based radar," *Waves in Random and Complex Media*, (14) 2, S189 - S273, 2004.